



# Ultrathin glass fiber microprobe for electroporation of arbitrary selected cell groups

Julita Kulbacka<sup>a,\*</sup>, Rafał Kasztelan<sup>b,c</sup>, Małgorzata Kotulska<sup>d</sup>, Dariusz Pysz<sup>b</sup>, Grzegorz Stępniewski<sup>b,c</sup>, Ryszard Stępień<sup>b</sup>, Jolanta Saczko<sup>a</sup>, Damijan Miklavčič<sup>e</sup>, Ryszard Buczyński<sup>b,c,\*</sup>

<sup>a</sup> Department of Molecular and Cellular Biology, Faculty of Pharmacy, Wrocław Medical University, Borowska 211A, 50-556, Wrocław, Poland

<sup>b</sup> Department of Glass, Institute of Electronic Materials Technology, Wolczyńska 133, 01-919, Warsaw, Poland

<sup>c</sup> Faculty of Physics, Warsaw University, Pasteura 7, 02-093 Warsaw Poland

<sup>d</sup> Department of Biomedical Engineering, Faculty of Fundamental Problems of Technology, Wrocław University of Science and Technology, Wybrzeże Wyspiańskiego 27, 50-370 Wrocław, Poland

<sup>e</sup> University of Ljubljana, Faculty of Electrical Engineering, Trzaska 25, SI-1000 Ljubljana, Slovenia

## ARTICLE INFO

### Article history:

Received 27 October 2019

Received in revised form 22 April 2020

Accepted 29 April 2020

Available online 13 May 2020

### Keywords:

Electroporation

Optical fibers

Electrochemotherapy

Microprobe

Drug delivery

## ABSTRACT

A new type of ultrathin fiber microprobe for selective electroporation is reported. The microprobe is 10 cm long and has a diameter of 350  $\mu\text{m}$ . This microprobe is a low cost tool, which allows electroporation of an arbitrary selected single cell or groups of cells among population with use of a standard microscope and cell culture plates. The microprobe in its basic form contains two metal microelectrodes made of a silver-copper alloy, running along the fiber, each with a diameter of 23  $\mu\text{m}$ . The probe was tested *in vitro* on a population of normal and cancer cells. Successful targeted electroporation was observed by means of accumulation of trypan blue (TB) dye marker in the cell. The electroporation phenomenon was also verified with propidium iodide and Annexin V in fluorescent microscopy.

© 2020 The Authors. Published by Elsevier B.V. This is an open access article under the CC BY-NC-ND license (<http://creativecommons.org/licenses/by-nc-nd/4.0/>).

## 1. Introduction

Lipid membranes isolate the interior of cells from the external environment and separate intracellular organelles. The application of electric fields with adequately high amplitude can lead to electroporation (EP) of cells. Electroporation is manifested as transiently increased membrane permeability that can resolve, resulting in cell survival (reversible electroporation) or can lead to cell death (irreversible electroporation). It has also been observed that under some conditions including e.g. large field magnitudes - cells can undergo lysis [7]. However, a reversible process also induces significant disturbance of cell homeostasis due to the increased influx of external molecules [8]. This process has been confirmed on various cell and artificial lipid models [9,10]. In addition to pore formation, other phenomena such as tubules and vesicles have been reported on giant unilamellar vesicles (GUV) [11]. Other methods that can reorganize lipid membranes have also been discovered which are based on optical membrane disruption, e.g. photoporation, optoinjection or laserfection [12,13]. The phe-

nomenon of temporary membrane permeabilization enables transport of hydrophilic molecules into the cell, which has been used in medicine and biotechnology for introduction of DNA, anticancer drugs and other small molecules [1-6]. Despite growing number of EP applications, its mechanisms are not yet fully elucidated. Studies of electroporation are mainly performed in bulk - on cell culture populations or *in vivo*. In both cases the results are derived from an ensemble of cells, which results in averaging of the phenomena occurring in the cells. It has been confirmed that individual cell entities can display significant variability [14,15]. Rare events occurring in heterogeneous cells can be obscured by the averaging effect. Additionally, cell culture resuspensions, involved in the bulk electroporation protocols, may significantly affect the cells state and viability, e.g. in post-mitotic cells, introducing undesirable artefacts to the experiment.

Observation of a single cell electroporation could improve our knowledge concerning the mechanisms of electroporation and its effects [16]. Delivery of electric field pulses to bulk tissue inevitably induces local thermal effect due to electric pulse delivery [17]. Therefore, single cell approaches can contribute to eliminating these effects on the surrounding cells and to decreasing of Joule heating. Among other possible experiments, different customized electroporation protocols could be performed on individual cells

\* Corresponding authors.

E-mail addresses: [julita.kulbacka@umed.wroc.pl](mailto:julita.kulbacka@umed.wroc.pl) (J. Kulbacka), [ryszard.buczynski@fuw.edu.pl](mailto:ryszard.buczynski@fuw.edu.pl) (R. Buczyński).

or on groups of cells in the same environment. For example, very few attempts have been undertaken to explain the initialization of the electroporation process with the current-clamp stimulus, which shows a much broader picture of the phenomenon [5,6,18]. Numerous studies require single-cell electroporation, in which electrical stimulus is supplied individually with a microprobe. Other possible experiments involve research with rare or expensive drugs, whose volumes could be significantly reduced with this approach.

Up to now a number of approaches have been proposed for single cell electroporation [15,19–26]. In the single-cell electroporation, a localized electric field is applied either to a single adjacent cell or to a small colony of cells, or to a cell in a microfluidic suspension. The field is delivered through a microfabricated device, while neighboring cells are exposed to very low intensity of the field or to no field at all. Lundqvist et al. (1998) first demonstrated single-cell electroporation using carbon-fiber microelectrodes [21]. Since then, other single-cell electroporation techniques have been developed using electrolyte-filled capillaries [27], micropipettes [28], microfabricated chips with electrode arrays [25,29,30], and multiwall carbon nanotubes [31]. Bae et al. (2006) applied single-cell electroporation to bovine endothelial cells in the patch clamp method [25]. Chang et al. (2009) studied genetic transfection of neural cells using a microelectrode array featuring thickened microelectrodes with vertical sidewalls, to focus electrical fields horizontally to the targets positioned in between paired electrodes. These microelectrodes were fabricated using gold electroplating, which was molded by photolithographically patterned SU-8 photoresist [26]. A similar technique was exploited by Santra et al. (2014), who used transparent indium tin oxide-based nanoelectrodes with SiO<sub>2</sub> layer reducing thermal effects and ion generation. The microchip was applied to single-cell electroporation on HeLa cells, allowing for delivery of quantum dots, dyes, and plasmids localized to area of the electrodes edge within 2 μm × 50 nm [32,33]. A microchip with nanochannels was proposed by Chang et al. [34]. This microplatform enabled simultaneous cell electroporation and dosage control, as well as high-throughput cell transfection. A multifunctional pipette to electroporate single cells individually and to locally deliver an analyte to glioma cell, was presented by Ainla et al. (2012) [35]. They used low resistance metallic electrodes. Most of the methods mentioned above however require dedicated devices for cell placement or a complex manipulation system. Moreover, most of these methods do not provide flexibility of the electrodes which could enable their desired placement with regard to the cell geometry, both in vitro (2D and 3D models) and *in vivo*.

The new single-cell approach that we present, will allow observing the phenomenon of electroporation in real time and in different experimental conditions, with regard to the type and morphological structure of the cell, characteristics of the microelectrode probe and electrical stimuli in vitro. Transport properties of cell membranes are important from the point of view of treatments which depend on intracellular concentrations. Choosing optimal parameters of electroporation in electrochemotherapy, IRE (irreversible electroporation - soft tissue ablation) or immunogene therapy will be possible only when the mechanisms of electroporation, as well as the structural and transport changes of membranes, are more precisely understood.

Previously, fiber optics technology was used as tools to deliver laser signal and molecules dispersed in solvents to tissues, as well as to acquire fluorescent signals in in-vitro and in-vivo systems [36,37]. A fiber optic microneedle device was used to deliver single-walled carbon nanohorns and increase the volumetric dispersal of macromolecules, when simultaneously stimulated with co-delivered laser beam into brain tumor models [38,39]. High-quality fluorescent image transmission was recently reported in

implantable fiberscopes, developed with flexible imaging bundles composed of 6000 individual channels [40]. However, no solution has been reported for integration of metal electrodes within flexible glass optical fibers.

In our current study we demonstrate a new fiber microprobe, which can be used for single-cell studies requiring application of electric field. The microprobe consists of two low-resistant silver-copper microelectrodes, separated 31 μm from each other, each with a diameter of 23 μm. The microelectrodes were covered with a glass fiber which was 352 μm in diameter (Fig. 1). For experiment some glass was removed at the end of the fiber to open 2 mm long electrodes. The open ends of the electrodes were further mechanically separated 210 μm from each other. The fiber microprobe's total longitudinal dimension of 10–30 cm allows easy penetration into a biological sample and its convenient manipulation, as previously reported [41]. We applied the probe to single-cell electroporation on two normal cell lines – CHO-K1 hamster ovarian fibroblasts – lacking ion channels, H9C2 rat myocardial cells and to two human cancer cell lines: LoVo (colon adenocarcinoma) and A431 (squamous carcinoma). For verification of microprobe efficiency, we designed experiments for verification in two stages: constant and pulsed electric field with the voltage up to 10 V was used (which corresponds to voltage-to-distance ratio of 476 V/cm). It allowed successful electroporation of a small, selected group of cells, as well as of single selected cells.

## 2. Materials and methods

### 2.1. Fabrication of the microprobe for electroporation

The microprobe is composed of two long metal microelectrodes incorporated into a glass fiber. For the development of the microprobe we used the stack-and-draw method commonly used for photonic crystal fiber development [42]. The method is based on initial preform development – stacking of macroscopic elements: glass rods and capillaries, metal wires – and further fusion and scaling down in a high temperature fiber drawing process (Fig. 2).

In the first step, we prepared a preform composed of glass rods and glass capillaries with metal wires (Fig. 2). For this purpose, we used a borosilicate glass labelled SK222 developed at Krosno Glassworks Corp. Poland. The glass rods and capillaries had an outer diameter of 3 mm, while inner diameter of the capillaries was 2 mm (Fig. 2).

In order to develop the electrodes, we used a silver-copper alloy wire labelled AgCu1. The composition of this alloy was chosen so

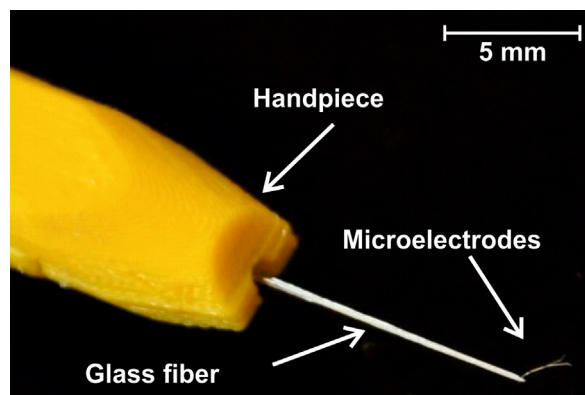


**Fig. 1.** Thin glass fiber microprobe for electroporation of selected cells. The probe contains two low-resistant silver-copper microelectrodes, separated 31 μm from each other, each with a diameter of 23 μm covered with a glass fiber with a diameter of 352 μm.

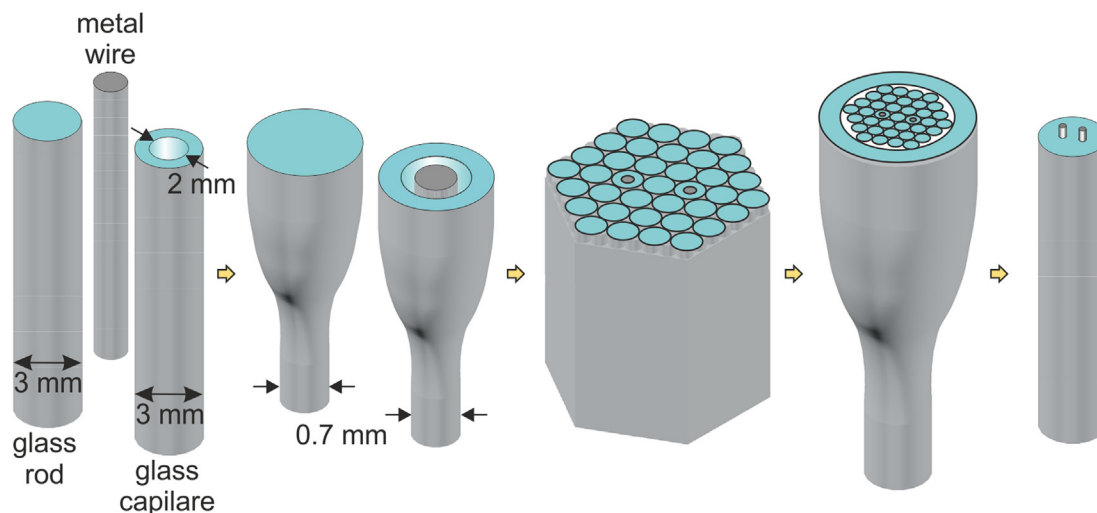


Fig. 2. Schematic of the stack-and-draw method used for microprobe development.

that the melting point of the alloy was lower by about 50 °C than the temperature drawing temperature of the SK222 glass. This ensures that the metal is in a liquid state during the fiber drawing process and enables formation of continuous electrodes (no discontinuities of the metal wires inside the glass fiber). The relatively high thermal expansion coefficient of glass ( $89 \times 10^{-7} \text{K}^{-1}$  @ 20–450 °C) reduces the stress on the glass-metal boundary. The thermo-physical properties of SK222 glass and AgCu1 alloy are presented in Tables 1 and 2 respectively.

The polished and degreased alloy rod was placed in a sealed SK222 glass capillary. The capillary was pumped off and flushed several times with argon before drawing down to remove oxygen and prevent oxidation of the metal. The fiber drawing process is performed in a protective atmosphere (argon) within the capillary. The developed glass rods (with metal cores) had an outer diameter in the range of 0.7 mm (Figs. 2 and 3). The structure of the microprobe preform consisted of two SK222 glass capillaries with metal rods inside, having a diameter of 0.7 mm and several SK222 glass rods with the same diameter of 0.7 mm. (Figs. 2 and 4). The whole structure was placed in the SK222 glass tube (Fig. 2). Total length of the preform was 250 mm. In the last stage the preform is drawn with the fiber drawing tower and scaled down to the required transverse dimensions (Fig. 2).

Prepared preforms were drawn at the fiber drawing tower, ensuring oxygen-free atmosphere inside the preform. During the drawing process all elements melted together and created a solid glass fiber with two continuous electrodes along its length. By changing the drawing conditions, such as feed and pulling rates, the thickness of the microprobe and of the inner electrodes could be controlled. We have verified experimentally feasibility of developing microprobe structures with various outer diameter in the range of 0.3 ÷ 0.5 mm. The lengths of developed microprobe fibers were in the range of 1 ÷ 50 m. However, there are no fundamental limits to further reduction of the microprobe's diameter, down to 100 μm and increase of length up to several hundred meters, when identical geometrical parameters are maintained. Ultimately, we

Table 1  
Properties of the AgCu1 alloy.

Parameter	alloy AgCu1
Melting point (°C):	620–650
Density (g/cm <sup>3</sup> )	9.4
Tensile strength (kg/mm <sup>2</sup> )	48

Table 2  
Properties of the SK222 glass.

Parameter	SK222
Refractive index $n_D$	1.520
The linear thermal expansion coefficient for a range of:	
20 ÷ 300 °C ( $10^{-7} \text{K}^{-1}$ )	84.0
20 ÷ 450 °C ( $10^{-7} \text{K}^{-1}$ )	89.0
Transition temperature $T_g$ (°C)	542
Dilatometric softening temperature DTM (°C)	610
Characteristic temperatures in the heating Leitz microscope:	
Temperature (°C)	
- Curvature	700
- Sphere	820
- Semisphere	950

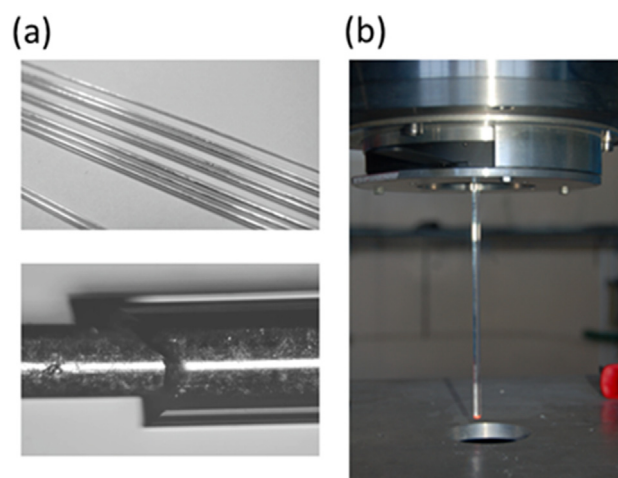
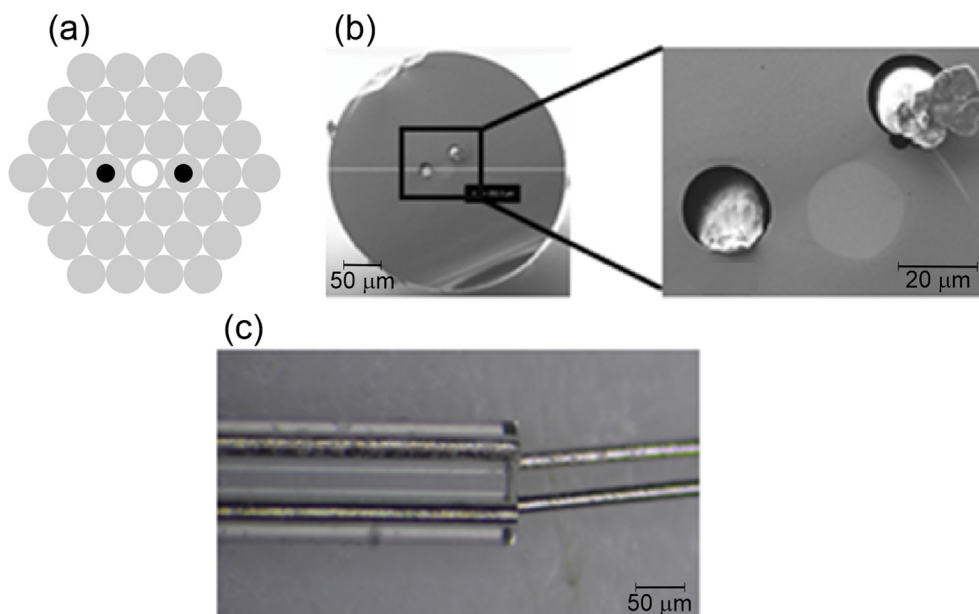


Fig. 3. Fabrication of the microprobe: (a) glass rods with metal core; (b) thermal pulling of the fiber with electrodes at fiber drawing tower.

have developed two series of microprobes, each 50 m long with outer diameters of 458 μm and 352 μm, respectively. Geometrical parameters of two series of microprobes are shown in Table 3. The cross-section of the microprobes with two metal electrodes is presented in Fig. 4b. The probe with a diameter of 352 μm contains two microelectrodes with diameters of about 23 μm. The stack-and-draw method is a mature fiber drawing technology. It is dedicated to developing at least hundreds of meters of fibers with



**Fig. 4.** Microprobe construction: (a) a scheme of preform for development of microprobe with two electrodes and high refractive index glass rods; (b) and (c) the cross-sections of microprobes with two metal electrodes (images obtained with a scanning electron microscope).

**Table 3**  
Summary of parameters of developer microprobes.

	GM1A/2	GM1A/3
The outer diameter ( $\mu\text{m}$ )	458	352
Electrode diameters ( $\mu\text{m}$ )	29/28	21/20
The distance between the electrodes ( $\mu\text{m}$ )	37	31
The diameter of the fiber ( $\mu\text{m}$ )	28	23

identical geometrical parameters from a single fiber preform. The parameters in this context would include the fiber diameter and the diameters of its internal components, such as air holes or electrodes.

## 2.2. Quality of the fiber microprobe

We verified quality of the microelectrodes using optical microscope and by measuring resistance of the microprobe samples. Samples with lengths of over 2 m and continuous metal wires (without longitudinal breaks or gaps) were successfully obtained, which enables to consider them for a practical application in electroporation. However, it is important to note that usually samples longer than 5 cm are not needed for *in-vitro* single-cell electroporation and samples longer than 20 cm are not needed for potential future applications in *in-vivo* electroporation. The fiber microprobe was cut into 10 cm long samples and metal electrodes were exposed at both ends of the probes to chemical etching in hydrofluoric acid. 30 min of etching in 20% solvent of hydrofluoric acid was optimal to fully etch the glass, while two metal electrodes remained undamaged.

We measured resistance of the microelectrodes using a probe station to determine their conductivity. We directly measured resistance in over 20 samples of each type of microprobes labelled GM1A/2 and GM1A/3 with individual lengths of 10 cm. Measured resistance was  $34 \pm 3 \Omega$  for a GM1A/3 fibers (electrodes with the diameter of 23  $\mu\text{m}$ ) and  $26 \pm 3 \Omega$  for a GM1A/2 fibers (electrodes with the diameter of 28  $\mu\text{m}$ ) (Fig. 5). The measured resistance difference between each type of samples depended mainly on the quality of electrical contact between the probe and microelec-

trodes. The measurement results confirmed low resistance of microelectrodes and proved good quality of all microelectrodes along the samples. Therefore, microelectrodes allowed to efficiently generate electrical potential between them. Moreover, generation of short, i.e. submillisecond electric pulses useful in some electroporation techniques is also possible. We have used the fiber microprobe for successful application of 100  $\mu\text{s}$  long pulses with 1 Hz repetition rate as shown in Section 2.7.

Finally, microelectrodes were connected to standard electrical wires to enable connection with a power source. For this purpose, the microprobe was mounted on a support plate. This approach allowed for building of rigid tips for both electrical connections and for manipulation during the experiments. The microprobe was attached to the support plate that provided electrical pads, using an epoxy adhesive. In the next step, microelectrodes were bonded to a macroscopic electric wire by means of conductive adhesive glue. Microelectrodes were precisely bonded with macroscopic electric wires under a microscope. Since microelectrodes were placed close to each other, there was the risk of breakdown when voltage was applied. Breakdown tests were performed in a saturated water solution of sodium chloride at room temperature (concentration of 26.5%). A power supply with control in the range of 0 ÷ 30 V was used. The tests showed negative results, which means that the breakdown voltage was higher than 30 V.

To verify flexibility of the fiber microprobes, we measured bending radius for 5 loops. We measured minimum acceptable bending radius of 5 cm for the fiber microprobe, which we used in the experiments. Based on further experiments with dummy fibers (no electrodes), further reduction of the microprobe diameter down to 100  $\mu\text{m}$  allowed to reduce its bending radius down to 1 cm.

## 2.3. Modeling of the electric field distribution

Simulations of electric field distribution are based on 2D and 3D finite element model (FEM) implemented in the COMSOL Multiphysics software package. The model assumes that resistance of the electrodes is based on experimental measurement data (26  $\Omega$  or 34  $\Omega$ ). The electrodes are immersed in a homogeneous medium

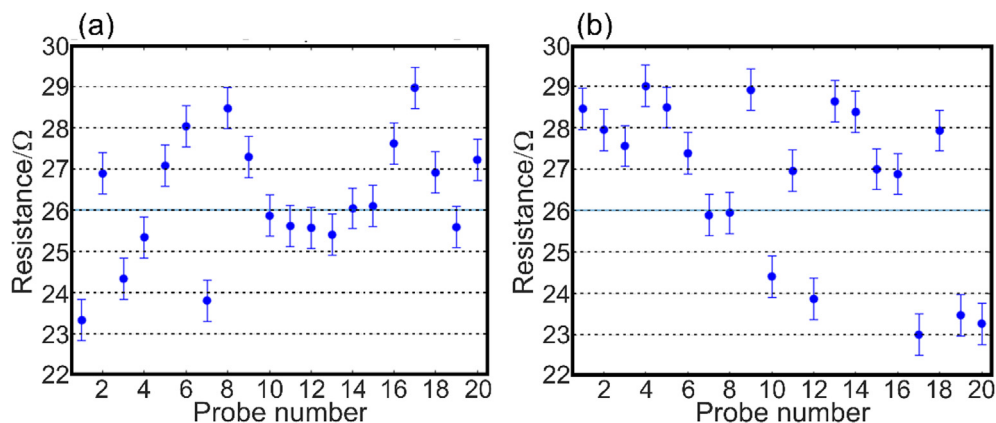


**Fig. 5.** Measurement results of electrode resistance in 10 cm long samples of two types of the fiber probes (a) GM1A/2 with the electrodes diameter of 28  $\mu\text{m}$  and (b) GM1A/3 with the electrodes diameter of 23  $\mu\text{m}$ .

with relative permittivity  $\epsilon_r = 80.2$  from one side, and from the other side they are placed inside a glass tube of relative permittivity 4.2. The voltage is applied to the end of electrodes from glass side.

#### 2.4. Cell culture

Experiments were performed on hamster ovarian fibroblastoid (CHO-K1, ATCC, CCL-61) cell line, neonatal rat cardio myoblasts (H9C2, ATCC CRL 1446), human colon adenocarcinoma cells (LoVo, ATCC, CCL-229) and human epidermoid carcinoma cell line (A431, ATCC, CRL1555). CHO-K1 cells can be applied as a model for transmembrane transport studies with the pulsed electric field due to very low expression of endogenous ion channels [43]. The cell line was selected to model a study involving drug transport. Ovarian fibroblasts were grown in Ham's F-12 K (Kaighn's modification) medium (Gibco, Poland) with addition of 10% fetal bovine serum (FBS, HyClone, Poland) and antibiotics (streptomycin/penicillin; Sigma). H9C2 neonatal rat cardio myoblasts and A431 cells were grown in DMEM (Lonza) medium with addition of 10% foetal bovine serum (FBS, Lonza), 2 mM Glutamine and 100x penicillin/streptomycin (Sigma). LoVo cells were grown in Ham's F-12 medium (Gibco, Poland) with addition of 10% fetal bovine serum (FBS, HyClone, Poland) and antibiotics (streptomycin/penicillin; Sigma). The cell lines were cultured in plastic flasks 25  $\text{cm}^2$  (Nunc, Denmark), which were stored in 37  $^\circ\text{C}$  and 5%  $\text{CO}_2$  in an incubator (SteriCult, ThermoScientific, Alab, Poland). For the experiments the cells were detached by trypsinization (Trypsin 0.025%; Sigma) and inactivated by cell specific culture medium, seeded on microscopic slides and dedicated for further experiments.

#### 2.5. Experimental setup for electroporation *in vitro*

Both cell lines were seeded on the superfrost basic microscopic slides (Thermo Scientific) and left overnight in 37  $^\circ\text{C}$  and 5%  $\text{CO}_2$  in an incubator. Then the cell lines were intended for single cell electroporation to verify EP phenomenon with the microprobes. We have used a standard setup for experiments composed of microscope (Olympus, CX41, Japan) with digital camera (Olympus SC30, 3.3 mln pixels) and standard cover slides (TB staining) or microscopic slides (fluorescent staining) (Fig. 6). The fiber microprobe was placed in a custom made arm mini-holder and manipulated. For this purpose, standard manual optomechanics was applied, including a 3-axis linear translation stage (Thorlabs, USA) with differential micrometer driver screws of 50 nm resolution. The end with the uncovered metal microelectrodes was

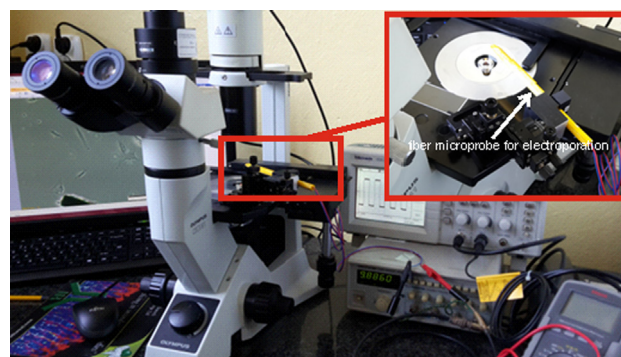


**Fig. 6.** Experimental setup used for electroporation of selected cells.

aligned and placed into cell plates under 20 $^\circ$  with respect to the cell plate surface to touch the surface of water film in the proximity of a cell to be electroporated.

#### 2.6. Electroporation with constant voltage

In this experiment the fiber microprobe labelled GM1A/2 was used. Since uncovered microelectrodes are flexible, we expanded the distance between them up to 220  $\mu\text{m}$ . It allowed us to perform electroporation on a selected group of cells placed between the ends of electrodes among all the population on the cell plate. Constant voltage in the range of 5  $\div$  9 V was applied for 3 min. Trypan blue (TB) dye (BioRad, Poland) was used as a marker of cell electroporation [44]. For intravital staining was used TB in PBS solution diluted 1:1. First electrical stimulation was initiated and, simultaneously with electric field, the TB dye solution was added by pipetting into the cell on the cover microscopic slide. Intravital observations were performed. Normally, TB is used to quantify live/dead cells, because it cannot penetrate membranes of living cells. Within the first minutes of our experiment, the dye entered only the cells, which membranes were affected by the electric field, and stained the nuclei in those cells. Due to the fact of relatively high cytotoxicity of Trypan Blue dye, which could affect cells strongly after exposition, the observations after staining were sustained no longer than 20 min., since TB was applied. The experiments were performed under a standard inverted contrast-phase microscopy (CX41 Olympus, Japan) using 100  $\times$  or 200  $\times$  magnification. The occurrence of electroporation was confirmed by transition of the marker solution into the cells. Cells were considered as electroporated (cell membrane permeability

increase) if staining with blue color was observed. The experiment was performed at minimum 4 slides/day of each cell line, and repeated minimum three times independently. Statistical evaluation of the calculated stained TB cells was performed on basis of marking and calculation of electroporated cells among the treated group (Table 4). Evaluation was performed by Chi<sup>2</sup> method for  $P \leq 0.05$ . In each set of experiments, minimum 50 cells were calculated from minimum three independent EP treatments. The number of affected cells was given as the percentage of treated cells.

### 2.7. Electroporation with pulsed electric field (PEF)

Pulsed voltage was applied in amplitude range of 5 ÷ 15 V, with electroporation parameters: 8 pulses and 100  $\mu$ s with the frequency of 1 Hz, the distance between electrodes: 130 ÷ 220  $\mu$ m. For this purpose, we have used a standard laboratory function generator (FG-7202, Voltcraft, Wernberg, Germany). The pulsed conditions were monitored with an oscilloscope (Tektronix, TDS 1002). Simultaneously, with electric field the TB dye was first added into a cell on a cover slide. The observations were performed on living cells. These experiments were observed with a standard inverted microscope (CKX41, Olympus, Japan). The experiment was performed at minimum 4 slides/day of each cell line, and repeated minimum three times independently.

In the next stage Annexin V-FITC (BioVision, USA) and propidium iodide (PI, Sigma-Aldrich, Germany) were used as markers of permeabilization. In physiological conditions, phosphatidylserine (PS) is present on the inner side of the plasma membrane lipid bilayer. When PS is exposed outside the cell membrane it is also a proof that cells underwent electroporation. This is often pointed as the first marker of permeabilization process. Next when cell membrane is unsealed, PI can enter the cell [44–47]. The cells were visualized after fixation in 4% paraformaldehyde (Roth, Germany) and observed with the fluorescent microscope (BX53, Olympus, Japan). The experiment was performed at minimum 4 slides of each cell line from independent experiments.

## 3. Results and discussion

We demonstrated the effectiveness of newly developed microelectrodes and demonstrated successful electroporation normal and cancer cells with constant or pulsed electric fields.

### 3.1. Electroporation with constant voltage

Initially, we used constant voltage to verify if cells present in the vicinity of the microprobe are affected. Cells were previously prepared on microscopic slides. The observation and image registration were provided with the microscope operated in the bright field mode. First, two normal cell lines CHO-K1 and H9C2 were tested (Fig. 7). When constant voltage of 6 V was applied, the trypan blue (TB) dye accumulated inside a selected group of cells (Fig. 7b, c and e). Applied voltage of 6 V in case of considered experimental setup with the fiber microprobe with electrodes with thickness of 23  $\mu$ m separated by 31  $\mu$ m corresponds to electrical

field strength of 1.9 kV/cm in the area between the electrodes. Normally TB is undetectable at low concentrations but when the cell membrane is permeabilized the dye can enter and accumulate within the cell, and dark blue color becomes apparent. Therefore, with the application of the TB test, the electro-permeabilized area (monolayer of cells) can be readily visualized. It proved occurrence of electroporation. Further increase of voltage, up to 9 V, which corresponded to electrical field strength of 2.9 kV/cm in the area between the electrodes, resulted in permanent damage of cell lipid membrane and outflow of cytoplasm from the cell (Fig. 7c). The characteristic bubbles were reported as a response against the cell lysis [48]. Cells at a further distance from microelectrodes were not electroporated, as shown in Fig. 7f. During electroporation we observed cell membrane blebbing, which is a typical phenomenon for membrane permeabilization during electroporation process. This was previously described in standard electroporation protocols [49].

We have calculated electric field distribution generated by the microprobe to evaluate range and strength of electrical field that interacts with the cell population. Relatively uniform electric field is generated between the electrodes while field declines exponentially outside the electrodes, as shown in Fig. 8. Based on our model we estimate that electroporation occurs in the areas between electrodes and in radius of 5–15  $\mu$ m outside of electrodes (above 0.6 kV/cm - denoted as dark yellow and red area), if 6 V is applied to the electrodes (Fig. 9). Other authors also used low constant DC voltage (5–9 V) and observed electroporation phenomenon in a single cell within the microfluidic droplet [50].

### 3.2. Electroporation with pulsed electric field

Pulsed electric fields were used in the next stage of verification of our ultrathin microprobe. According to clinical electrochemotherapy, standard parameters of electroporation were applied, the same as in clinical procedures: 8 pulses, 100  $\mu$ s with the repetition frequency of 1 Hz, and the voltage in the range of 5 ÷ 15 V, which corresponds to 0.22 – 1.0 kV/cm voltage-to-distance ratio, since the distance between open ends of the electrodes in case of these experiments varied between 150 and 230  $\mu$ m. In this evaluation model, normal cells CHO-K1 and also cancer cell lines (LoVo and A431) were treated. The results are presented in Fig. 10, which shows images obtained with the bright field microscope mode, and in Fig. 11, which shows results obtained by means of a fluorescent microscope. Cells showed symptoms of permeabilization for voltages above 10 V which corresponds to intensity of electrical field 440 V/cm. In CHO-K1 and LoVo cells cytoplasm outflow and characteristic bubbles were visible (Fig. 9a and b). Trypan blue staining also confirmed the presence of electroporation process in CHO-K1, A431 and LoVo cells (Fig. 10c). Only cells in the vicinity of the electrodes accumulated the blue dye. Because of relatively high cytotoxicity of TB, what implicates short observation time after electropulsation, we can state that electroporation occurs and assume that might be reversible, according to the parameters applied in the experiment with reference to the available data [2,3]. Khine et al. [24] also confirmed single cell electroporation using trypan blue assay, although the experiment was performed on a dedicated chip. The authors could trap the single cell on the chip and observe dye accumulation with low voltage at the level of 1 V [24]. Ghosh et al. [51] using voltage pulses (0.1–0.2 ms in duration) with electric field range: 5–7 V observed uptake of trypan blue into cells demonstrated that the plasma membrane is permeabilized by the delivery of a voltage pulse [51].

To verify relation between cell viability and electric field strength we have used equation that describes the probability for cell survival [52]:

**Table 4**  
The evaluation of the percentage of electroporated cells.

Cell lines	CHO-K1	LoVo	A431
Bright field observations (no dye)	10%±1.5	68%±3*	35%±2.5
Trypan blue staining	15%±2	86%±4*	43%±3
Fluorescent imaging	98%±1*	97%±2*	no data

\*  $P \leq 0.05$  (by Chi<sup>2</sup> method)

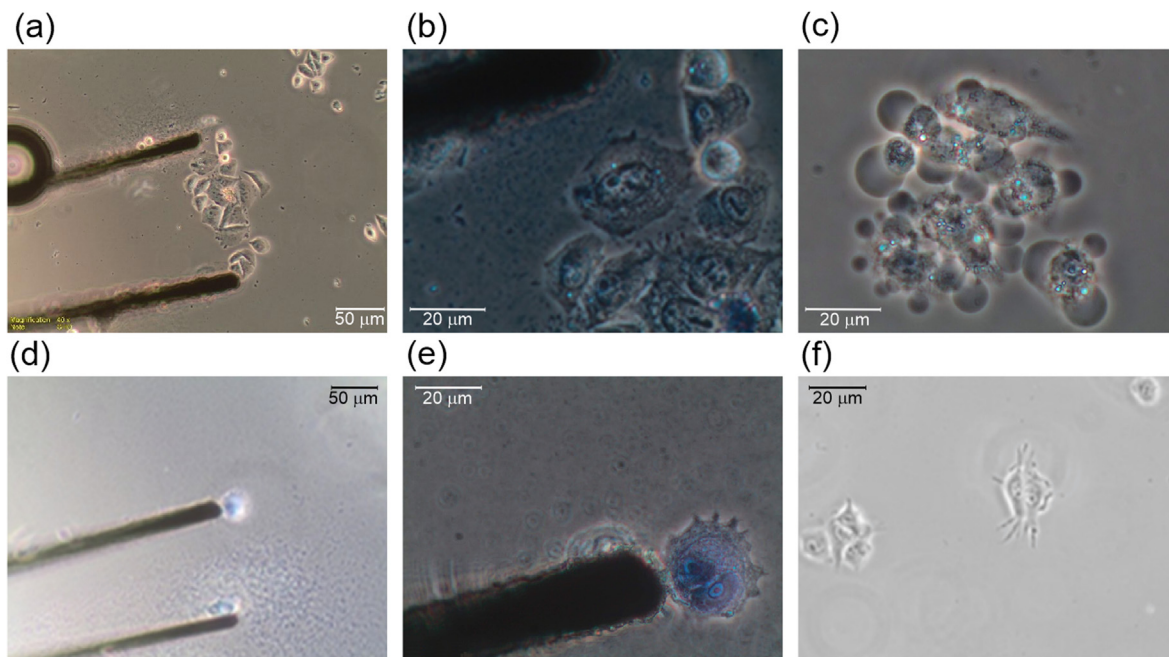


**Fig. 7.** Cell membrane permeabilization verification with trypan blue staining after electroporation, using the microprobe with constant voltage (6 V) on CHO-K1 (a) before exposing to electric field; (b) during electric field exposure; (c) after electric field exposure; and on H9C2 cells (d) during electric field exposition; (e) after electric field exposition; (f) unaffected cells at a distance from the electrodes. (For interpretation of the references to color in this figure legend, the reader is referred to the web version of this article.)

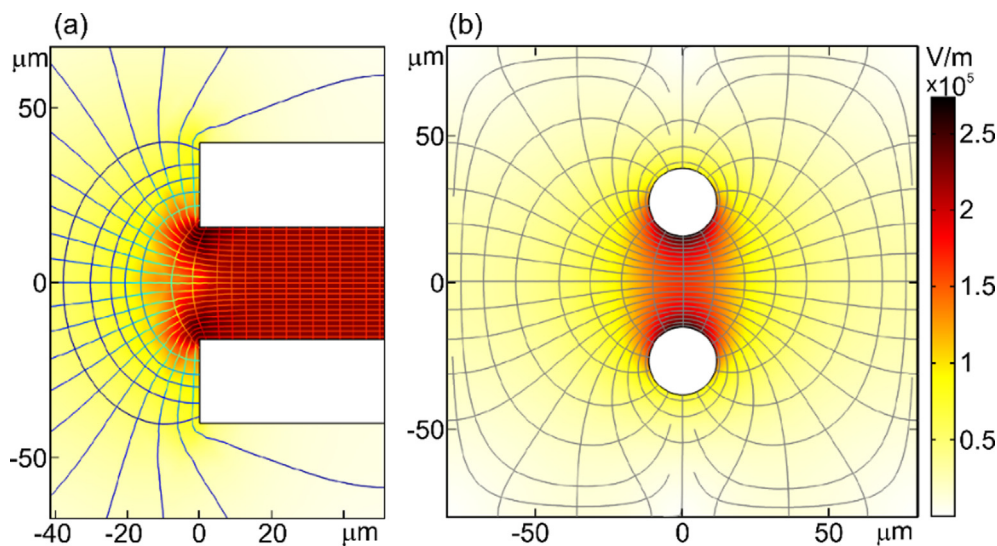


**Fig. 8.** Electric field intensity distribution (color), as well as electric field line (gray) for tested fiber microprobe labelled GM1A/3 with two microelectrodes of the diameter 23 μm each and for constant voltage 6 V applied: (a) an in-plane cross-section along electrodes, (b) cross-section in the plane perpendicular to the probe in the proximity of the end of the electrodes.

$$S(E, N) = \frac{1}{1 + \exp\left[\frac{E - E_c(N)}{A(N)}\right]} \quad (1)$$

where  $E$  denotes the electrical field,  $N$  is the number of pulses,  $E_c$  is the critical electric field, in which 50% of cells are killed, and  $A$  is a kinetic constant which defines curve slope.

In case of our model, we assumed 100 μs pulses with various voltage in the range 0–15 V, which corresponds to the electric field strength 0–362 V/cm for a single pulse (Fig. 12a). The available data indicate that similar parameters are effectively used for gene transfection and drug delivery [44]. Based on our model, we can conclude that for voltage below 4.5 V, the electroporation would

not occur. For the voltage range 4.5–7.1 V reversible electroporation occurs, while cell viability is reduced with an increased voltage till 9 V, where irreversible electroporation permanently damages all cells (Fig. 12b).

In a next step, evaluation was performed with fluorescent assay using Annexin V (PS maker, when externalized) and propidium iodide (PI). Similarly to TB assay, experimental observations indicated phosphatidylserine (PS) externalization. PS staining was combined with the propidium iodide (PI) uptake, which is an impermeable dye. When cells were exposed to electric pulses (10 V), as shown in Fig. 11, the continuity of the cell membrane was affected, what was represented as red fluorescence. Obtained

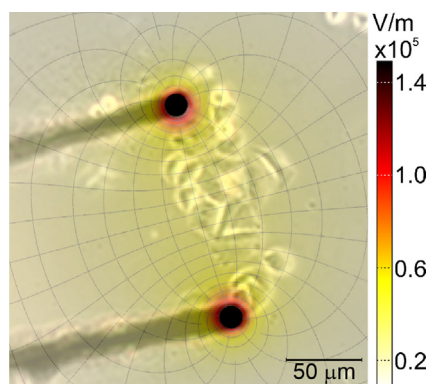


**Fig. 9.** Overlap between measured electroporated CHO-K1 cells and modelled electric field distribution for tested fiber microprobe labelled GM1A/3, with two microelectrodes of the diameter 23  $\mu\text{m}$ , if 6 V external voltage is applied.

results prove the membrane electroporation in treated cell lines. The method with phosphatidylserine (PS) externalization is used for indication of the membrane permeabilization, when observed shortly after cell expose to electric field [44].

### 3.3. Prospects for *in-vivo* applications

Electroporation as a medical treatment is already used as a support therapy in case of several types of cancer [53–56], but the available tools enable only bulk tissue medical treatments. In previous section have only verified the fiber microprobe for selective cell electroporation in *in vitro* systems. However, the proposed technology has a large potential also for future *in-vivo* applications, although these applications require additional studies. Since our proposed microprobe for electroporation has a form of a fiber, it can be considered in future for *in vivo* medical treatment of a small-area, difficult to access glioma, pancreatic cancers or during endoscopic procedures e.g. bronchoscopy for treating (small) lung metastasis. Below we discuss shortly technological prospects to meet various requirements for *in-vivo* applications.

The stack-and-draw fiber technology allows integration of additional functionalities in a single fiber microprobe as a drug delivery channel, illumination and imaging channels, which further extend its future application capabilities as a new medical tool for *in-vivo* selective treatment of internal organs (Fig. 13a).

In particular, the single fiber microprobe can also contain a microchannel for local medical delivery integrated with an optofluidic pump. The microchannel will allow high dosage control, as well as minimal amounts of the compounds - providing a useful method for rare or expensive agents. Another potential application is studying cells, in which delivery of a highly localized electrical stimulus is needed, for example limited to a single axon in neural cells. Importantly, our probe can contain a microchannel along the electrodes, allowing for local delivery of experimental drugs or other compounds. The probe can also deliver localized light, which can be used for activating biochemical processes, e.g. in photodynamic reaction in cancer cells, remove some tissues with suction channel and enable visualization (with imaging channel) of the field in front of the electrodes. Moreover, in the future, the ultra-thin microprobe can be also widely applied in dermatology and esthetic surgery applications, where precise targeting of deep skin layers and active substance delivery and stimulation is required. Additionally, minimal scarring is possible.

We have also successfully developed a microprobe with an integrated delivery channel (Fig. 13b). We developed a fiber with 2 electrodes with the diameter of 65  $\mu\text{m}$ , each and central air channel with a diameter of 90  $\mu\text{m}$ . This fiber microprobe contains also two high refractive index cores for simultaneous delivery and detection of optical signals. The core diameter is 72  $\mu\text{m}$ . Total diameter of the fiber microprobe is 422  $\mu\text{m}$  and can be further scaled up or down, according to application requirements. Microchannel can ensure good localization of drug delivery, but dosage control will depend on both microchannel diameter and pump control system. To control dosage, we used a micropump system of Fluigent MFCS™-EZ pump supplemented by flow-rate platform [57]. Typically, this microfluidic pump offer flows in the range from 7.5 nL/min to 5 ml/min with accuracy better than 1%. The new microprobe was however not verified experimentally for electroporation, since simultaneous connection of electrodes and drug delivery channel with an external electrical supplier and a microfluidic pump,

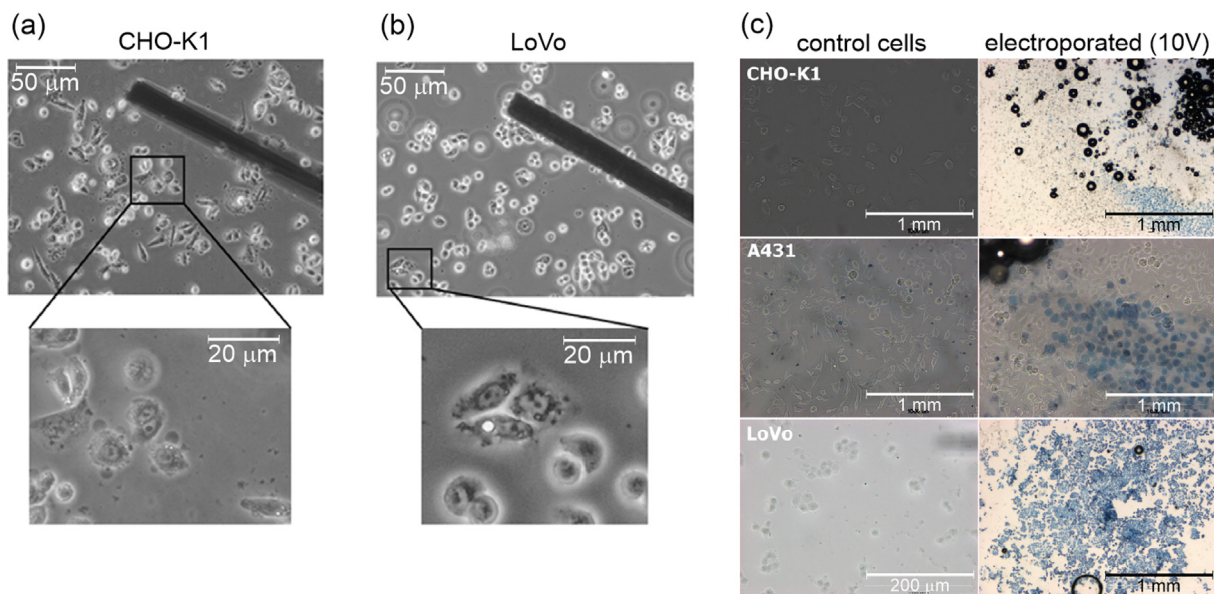


**Fig. 10.** The evaluation of the electroporation process using microprobe with pulsed electric field (8 pulses, 100  $\mu\text{s}$ , 1 Hz, 10 V) in (a) CHO-K1; (b) LoVo cells and (c) trypan blue staining in CHO-K1, A431 and LoVo cells visualized by bright field microscope. Stained-affected cells near the electrodes. (For interpretation of the references to color in this figure legend, the reader is referred to the web version of this article.)

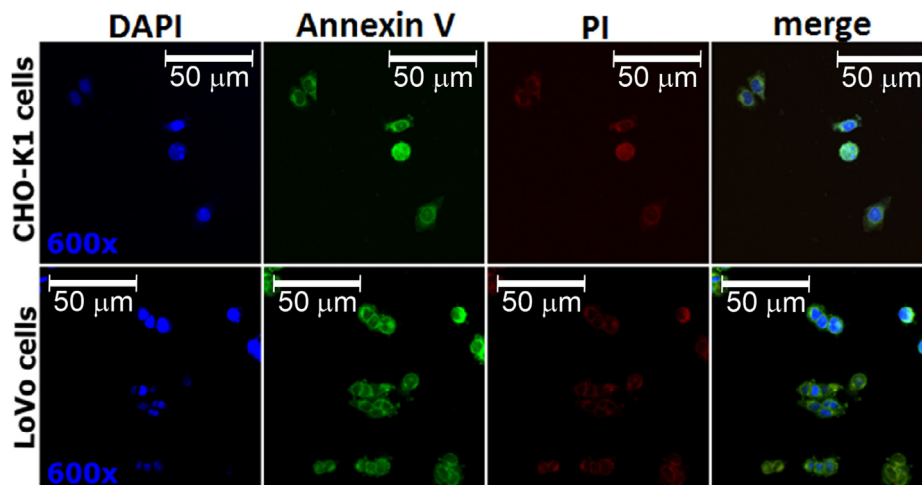


**Fig. 11.** Evaluation of the microprobe electroporation process using microprobe with pulsed electric field (8 pulses, 100 μs, 1 Hz, 10 V) in CHO-K1 and LoVo cells. Cellular nuclei were stained with DAPI; phosphatidylserine (PS) externalization was determined by Annexin-V-FITC, cell membrane unsealing was marked with propidium iodide (PI) and visualized by a fluorescent microscope.

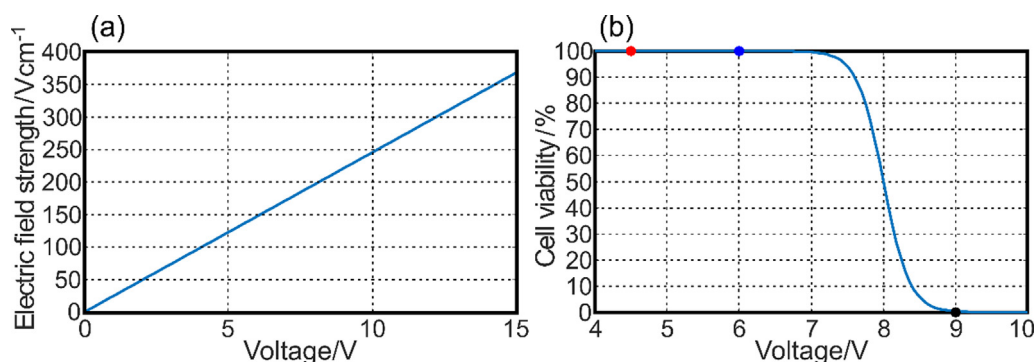


**Fig. 12.** Probability for cell survival for various voltage values applied to the fiber microprobe; (a) electric field strength for the area between the electrodes when voltage is applied to the fiber microprobe labelled GM1A/3 with two microelectrodes of diameter of 23 μm; (b) cell viability for various voltage applied. Red dot denote area where cell is not electroporated, blue dot –reversible electroporation occurs, black dot – all cells are permanently damaged/irreversible electroporation. (For interpretation of the references to color in this figure legend, the reader is referred to the web version of this article.)

respectively, is not trivial. We have tested flow with the fiber microprobe with a microchannel and with inner diameters of 90 μm. We tested the flow rate from 100 nl/min to 3 μl/min and obtained a flow stability control of approx. 1%.

The microprobe we used for single cell electroporation has very limited area where electrical field is created. Our proposed approach offers scalability of this area with electrode multiplication. This way, with interleaved electrical potential distributed between several electrodes, an area of electroporation can be increased, while applied voltage remains low to limit thermal effects. Technological tests proved a possibility to develop multiple electrodes within a single fiber microprobe (Fig. 13c). We developed a test fiber with 19 electrodes, each with diameter of 35 μm. The electrodes are ordered in a hexagonal lattice with the lattice pitch of 62 μm (Fig. 13d). Outer diameter of the fiber microprobe is 515 μm and can be further increased, if required. An increase of diameter of microprobe over diameter of 1 mm is not practical for potential applications with larger tumor size, but can be considered for application in treatments of small metastasis, which are not resectable or difficult to reach.

Recently we have developed a flexible imaging bundle with pixel size of 1.1 μm based on pair of silicate glasses with large refractive index difference [58]. The fiber bundle has a total diameter of 230 μm and it contains over 15,000 pixels (Fig. 13d). Due to small pixel size, a high-resolution imaging bundle a delivery

channel can be in the future integrated as a single microprobe with electrodes to open a route for imaging of the electroporated area. This solution might find unique application in electroporation of arbitrary selected cell groups in 3D cultures, since the fiber microprobe can address a selected cell among 3D culture, while the integrated imaging bundle ensures imaging of the surrounding area.

Currently, there are numerous solutions dedicated to observation of single cell phenomena including fundamentals of electroporation. However, the microprobe presented here, in comparison to others, seems to be more economic to develop and is supported by additional functionalities, such as channels for drug and light delivery, and also a fiber channel for image processing. Table 5 contains a summary comparison of the available single cell electroporation solutions.

#### 4. Conclusions

Results obtained in scope of this work indicate that the fiber microprobe with integrated microelectrodes has potential for applications in biotechnological and medical research. This would specifically involve cellular phenomena related to electrical stimulus of biological and artificial membranes. The demonstrated technological solution is precise and selective, thus it is less invasive, than existing technologies. It allows to deliver precisely selected

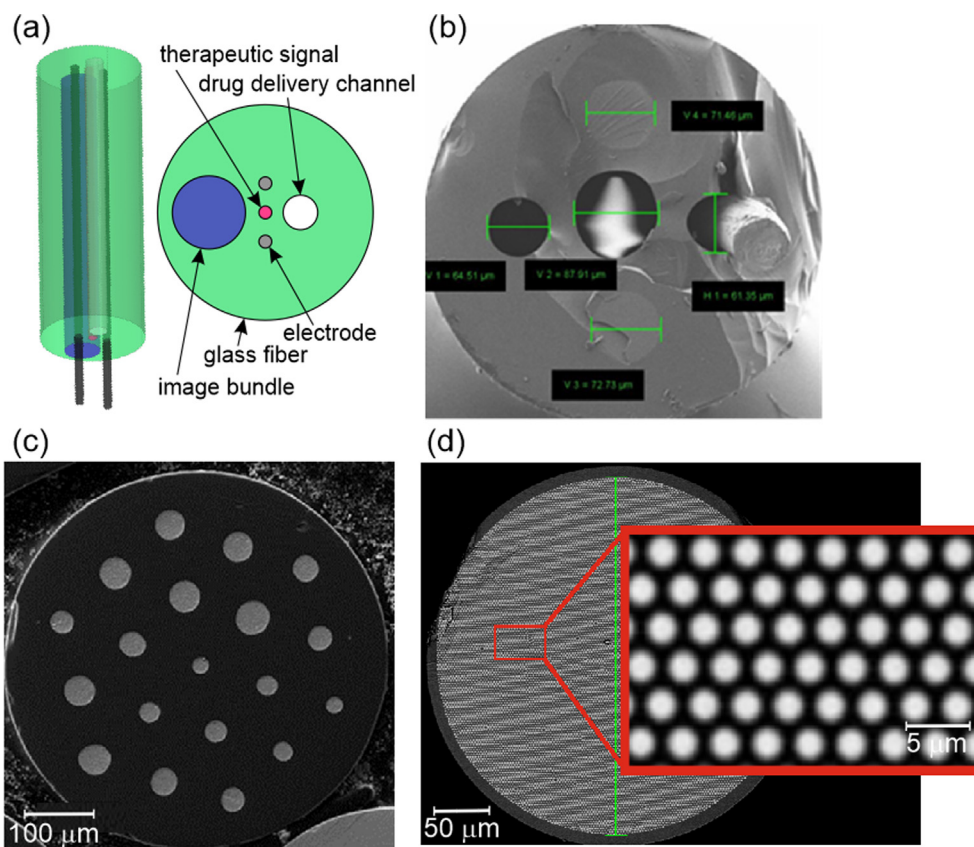


**Fig. 13.** Perspective for development of multifunctional fiber microprobe: (a) Schematic of a multifunctional fiber microprobe for electroporation; (b) a fabricated fiber microprobe with integrated drug delivery channel, optical signal channel and two electrodes; (c) a demonstration of a fiber microprobe with multiple electrodes; (d) and of imaging fiber with ultra-small high-aperture pixels.

**Table 5**

Comparison of available electroprobes for electroporation applications.

	Type of cells	Microscopic observations	Drug/gene delivery	Light delivery	Cell manipulation
Fiber microprobe (this paper)	Adherent cells	+	+	+	+
Lab-on-chip microfluidic system [30]	Cells in suspension	+	-	-	-
Multi-walled carbon nanotubes [31]	bacteria	+	-	-	No but targeted transport to the electroporated bacteria
Patch clamp-based microelectroporation [25]	Adherent cells	+	-	-	+
high-throughput in situ cell electroporation (HiCEP) microsystem [29]	Adherent cells	+	+	-	-
Electrolyte-filled Capillary [27]	Cells and tissues	+	+	-	+

electrical signal into arbitrary selected cell among the cell population.

The experiments can be carried out on adherent cells, eliminating the need of cell suspensions, centrifugation and trypsinization. Additionally, it allows for observation of phenomena which appear only in limited number of cells among a large population. Studies with the microprobe require very low voltages, at the level of few volts, while compared to the bulk methods, since the distance between the electrodes is very small. In this case, standard pulse generators can be applied. The precise delivery of the electric field does not affect cells at the distance and reduces heating effects. Flexibility of the fiber may enable arbitrary placement of the electrode, due to the cell geometry, in vitro systems. This application is not possible with already described methods, such as electrolyte-filled capillaries, micropipettes (patch-clamp electrodes), or chip structures. The flexibility of our microprobe is a consequence of

the fiber geometry – it may be long up to 30 cm with unbroken electrode structure, with the electrodes as small as 23  $\mu\text{m}$  in diameter, very close to each other (31  $\mu\text{m}$ ). The fiber geometry may enhance use of electroporation technique in laparoscopy and other *in vivo* techniques.

Additionally, the microchannel will allow precise dosage control, as well as minimal amounts of the treatment compounds - providing a useful method for rare or expensive agents. The microprobe can be used in water environment (a typical cell culture laboratory) without breakdown and destruction of samples or the microprobe. The microprobe can be used for *in-vitro* study of single or group cell analysis, and for specific cancer treatment of a small-area, such as the difficult to access glioma or pancreatic cancer. The *in-vitro* studies involve precise identification of the stimulus parameters needed for electroporation of specific cell types in situ, discovery of the relation between field parameters, arising

after EP membrane “nanopores” dimensions and conductivity. Possible studies are not limited to pulsed electric fields, currently used in electroporation of cells, but allow for constant current experiments. Research regarding single-cell electrochemotherapy, tissue ablation, DNA vaccination or genetic modifications are also feasible. The proposed microprobe implementation exceeds other solutions with the ease of fabrication and multitasking depending on the particular demand. However, the developed electrode is a proof-of-concept only and still requires further research to take full advantage of its technological possibilities.

### Declaration of Competing Interest

The authors declare the following financial interests/personal relationships which may be considered as potential competing interests: [Ryszard Buczyński, Dariusz Pysz and Ryszard Stępień are inventors of patents owned by Institute of Electronic Materials Technology in Warsaw in technical field of the publication].

### Acknowledgements

This work was supported by the Foundation for Polish Science, Poland, grant POIR.04.04.00-1C74/16, National Centre for Research and Development, Poland, grants TANGO 2/339928/NCBR/2017 and SONATA BIS (2016/22/E/NZ5/00671, COST Action TD1104 EP4Bio2Med).

The authors wish to acknowledge Dr. Z. Szczepanski from Warsaw University of Technology (Poland), for his support in microelectrode bonding, Mrs. I. Pietrzyk from University of Warsaw for support in microprobe integration. The authors thank Prof. Fluvio Ursini from University of Padua (Italy) for providing cell line of rat neonatal cardio myoblasts (H9C2) used for experiment. The authors are grateful to prof. Tom Vernier from Old Dominion University (Norfolk, VA, USA) for the insightful comments and suggestions to the performed research and manuscript.

### Author Contributions

R.B., D.P. and R.S. created a concept of the fiber microprobe. R.B. designed, D.P. and R.S. fabricated the microprobe. J.K. and J.S. planned the experiment. R.B. and G.S. built the experimental setup. J.K. and G.S. performed all the experimental work. R.K. performed modeling of electromagnetic field distribution. J.K. and J.S. processed all experimental data and analyzed all results. J.K., M.K. and R.B. wrote manuscript. J.S. and D.M. contributed to writing of the manuscript. J.K. and R.B. equally contributed to this manuscript.

### Appendix A. Supplementary material

Supplementary data to this article can be found online at <https://doi.org/10.1016/j.bioelechem.2020.107545>.

### References

- [1] A. Golberg, M. Sack, J. Teissie, G. Pataro, U. Pliquet, G. Saulis, S. Töpfl, D. Miklavčič, E. Vorobiev, W. Frey, Energy-efficient biomass processing with pulsed electric fields for bioeconomy and sustainable development, *Biotechnol. Biofuels* 9 (2016) 94.
- [2] T. Kotnik, W. Frey, M. Sack, S. Haberl Meglič, M. Peterka, D. Miklavčič, Electroporation-based applications in biotechnology, *Trends Biotechnol.* 33 (2015) 480–488.
- [3] M.L. Yarmush, A. Golberg, G. Serša, T. Kotnik, D. Miklavčič, Electroporation-based technologies for medicine: principles, applications, and challenges, *Annu. Rev. Biomed. Eng.* 16 (2014) 295–320.
- [4] G. Serša, J. Teissie, M. Čemažar, E. Signori, U. Kamenšek, G. Marshall, D. Miklavčič, Electrochemotherapy of tumors as in situ vaccination boosted by immunogene electrotransfer, *Cancer Immunol. Immunother.* 64 (2015) 1315–1327.
- [5] C. Jiang, R.V. Davalos, J.C. Bischof, A Review of Basic to Clinical Studies of Irreversible Electroporation Therapy, *IEEE Trans. Biomed. Eng.* 62 (1) (2015) 4–20.
- [6] L. Lambrecht, A. Lopes, S. Kos, G. Sersa, V. Prêat, G. Vandermeulen, Clinical potential of electroporation for gene therapy and DNA vaccine delivery, *Expert Opin. Drug Delivery* 13 (2) (2016) 295–310.
- [7] A. Ivorra, B. Rubinsky, Historical Review of Irreversible Electroporation in Medicine, *Irreversible Electroporation*. Springer, Berlin Heidelberg, 2010, pp. 1–21.
- [8] A.M. Bowman, O.M. Nesin, O.N. Pakhomova, A.G. Pakhomov, Analysis of plasma membrane integrity by fluorescent detection of Tl<sup>+</sup> uptake, *J. Membr. Biol.* 236 (1) (2010) 15–26.
- [9] D.L. Perrier, L. Rems, P.E. Boukany, Lipid vesicles in pulsed electric fields: Fundamental principles of the membrane response and its biomedical applications, *Adv. Colloid Interf. Sci.* 249 (2017) 248–271.
- [10] T. Kotnik, L. Rems, M. Tarek, D. Miklavčič, Membrane electroporation and electroporation: Mechanisms and models, *Annu. Rev. Biophys.* 48 (2019) 63–91.
- [11] T. Portet, F. Camps i Febrer, J. M. Escoffre, C. Favard, M. P. Rols, D. S. Dean, Visualization of membrane loss during the shrinkage of giant vesicles under electropulsation, *Biophys. J.* 96(10), 4109–21 (2009).
- [12] M.P. Stewart, R. Langer, K.F. Jensen, Intracellular delivery by membrane disruption: Mechanisms, strategies, and concepts, *Chem. Rev.* 118 (2018) 7409–7531.
- [13] K. Dhakal, B. Black, S. Mohanty, Introduction of impermeable actin-staining molecules to mammalian cells by optoporation, *Sci. Rep.* 4 (2014) 6553.
- [14] S.K. Frandsen, L. Gibot, M. Madi, J. Gehl, M.-P. Rols, Calcium Electroporation: Evidence for Differential Effects in Normal and Malignant Cell Lines, Evaluated in a 3D Spheroid Model, *PLoS ONE* 10 (12) (2015) e0144028.
- [15] C.J.W. Meulenber, V. Todorovic, M. Cemazar, Differential Cellular Effects of Electroporation and Electrochemotherapy in Monolayers of Human Microvascular Endothelial Cells, *PLoS ONE* 7 (12) (2012) e52713.
- [16] M. A. Chiapperino, L. Mescia, P. Bia, B. Staresinic, M. Cemazar, V. Novickij, A. Tabasnikov, S. Smith, J. Dermol-Cerne, D. Miklavcic, Experimental and Numerical Study of Electroporation Induced by Long Monopolar and Short Bipolar Pulses on Realistic 3D Irregularly Shaped Cells. *IEEE Trans. Biomed. Eng.* Year: 2020 | Early Access Article | Publisher: IEEE.
- [17] T. Forjanič, B. Markelc, M. Marčan, E. Bellard, F. Couillaud, M. Golzio, D. Miklavčič, Electroporation-induced stress response and its effect on gene electrotransfer efficacy: in vivo imaging and numerical modeling, *IEEE Trans. Biomed. Eng.* 66 (9) (2019) 2671–2683.
- [18] S. Koronkiewicz, S. Kalinowski, K. Bryl, Programmable chronopotentiometry as a tool for the study of electroporation and resealing of pores in bilayer lipid membranes, *Biochim Biophys Acta* 1561 (2) (2002) 222–229.
- [19] M. Kotulska, Natural Fluctuations of an Electropore Show Fractional Lévy Stable Motion, *Biophys. J.* 92 (7) (2007) 2412–2421.
- [20] M. Kotulska, J. Basalyga, M.B. Derylo, P. Sadowski, Metastable Pores at the Onset of Constant-Current Electroporation, *J. Membr. Biol.* 236 (1) (2010) 37–41.
- [21] J.A. Lundqvist, F. Sahlin, M.A. Aberg, A. Strömberg, P.S. Eriksson, O. Orwar, Altering the biochemical state of individual cultured cells and organelles with ultramicroelectrodes, *Proc Natl Acad Sci U S A.* 95 (18) (1998) 10356–10360.
- [22] F. Ryttsén, C. Farre, C. Brennan, S.G. Weber, K. Nolkranz, K. Jardemark, D.T. Chiu, O. Orwar, Characterization of single-cell electroporation by using patch-clamp and fluorescence microscopy, *Biophys. J.* 79 (4) (2000) 1993–2001.
- [23] J.L. Rae, R.A. Levis, Single-cell electroporation, *Pflügers Arch. - Eur. J. Physiol.* 443 (2002) 664–670.
- [24] M. Khine, A. Lau, C. Ionescu-Zanetti, J. Seo, L.P. Lee, A single cell electroporation chip, *Lab Chip* 5 (1) (2005) 38–43.
- [25] Ch. Bae, P.J. Butler, Automated single-cell electroporation, *Biotechniques* 41 (4) (2006) 399–402.
- [26] W.C. Chang, D.W. Sretavan, Single cell and neural process experimentation using laterally applied electrical fields between pairs of closely apposed microelectrodes with vertical sidewalls, *Biosens. Bioelectron.* 24 (12) (2009) 3600–3607.
- [27] K. Nolkranz, C. Farre, A. Brederlau, R.I.D. Karlsson, C. Brennan, P.S. Eriksson, S. G. Weber, M. Sandberg, O. Orwar, Electroporation of Single Cells and Tissues with an Electrolyte-filled Capillary, *Anal. Chem.* 73 (18) (2001) 4469–4477.
- [28] J.S. Wiegert, C.E. Gee, T.G. Oertner, Single-Cell Electroporation of Neurons, *Cold Spring Harb. Protoc.* 2 (2017), <https://doi.org/10.1101/pdb.prot094904>.
- [29] S. Bian, Y. Zhou, Y. Hu, J. Cheng, X. Chen, Y. Xu, P. Liu, High-throughput in situ cell electroporation microsystem for parallel delivery of single guide RNAs into mammalian cells, *Sci. Rep.* 7 (2017) 42512.
- [30] T. Geng, C. Lu, Microfluidic electroporation for cellular analysis and delivery, *Lab Chip* 13 (19) (2013) 3803–3821.
- [31] J. Rojas-Chapana, J. Troszczyńska, I. Firkowska, C. Morszeck, M. Giersig, Multi-walled carbon nanotubes for plasmid delivery into *Escherichia coli* cells, *Lab Chip* 5 (5) (2005) 536–539.
- [32] T. S. Santra F. G. Tseng, Recent Trends on Micro/Nanofluidic Single Cell Electroporation, *Micromachines* 4, 333–356 (2013).
- [33] T.S. Santra, H.Y. Chang, P.C. Wang, F.G. Tseng, Impact of pulse duration on localized single-cell nano-electroporation, *Analyst.* 13 (23) (2014) 6249–6258.
- [34] L. Chang, P. Bertani, D. Gallego-Perez, Z. Yang, F. Chen, C. Chiang, V. Malkoc, T. Kuang, K. Gao, L.J. Lee, W. Lu, 3D nanochannel electroporation for high-throughput cell transfection with high uniformity and dosage control, *Nanoscale* 8 (1) (2016) 243–252.

- [35] A. Ainla, S. Xu, N. Sanchez, G.D.M. Jeffries, A. Jesorka, Single-cell electroporation using a multifunctional pipette, *Lab Chip* 12 (2012) 4605–4609.
- [36] R.L. Hood, J.H. Rossmeisl, R.T. Andriani, A.R. Wilkinson, J.L. Robertson, C.G. Rylander, Intracranial hyperthermia through local photothermal heating with a fiberoptic microneedle device, *Lasers Surg. Med.* 5 (2013) 167–174.
- [37] M.S. Pochechuev, I.V. Fedotov, O.I. Ivashkina, M.A. Roshchina, D.V. Meshchankin, D.A. Sidorov-Biryukov, A.B. Fedotov, K.V. Anokhin, A.M. Zheltikov, Reconnectable fiberscopes for chronic in vivo deep-brain imaging, *J. Biophotonics* 11 (2018).
- [38] R.L. Hood, R.T. Andriani, S. Emch, J.L. Robertson, C.G. Rylander, J.H. Rossmeisl, Fiberoptic microneedle device facilitates volumetric infusate dispersion during convection-enhanced delivery in the brain, *Lasers Surg. Med.* 45 (2013) 418–426.
- [39] R.L. Hood, W.F. Carswell, A. Rodgers, M.A. Kosoglu, M.N. Rylander, D. Grant, J.L. Robertson, C.G. Rylander, Spatially controlled photothermal heating of bladder tissue through single-walled carbon nanohorns delivered with a fiberoptic microneedle device, *Lasers Med. Sci.* 28 (2013) 1143–1150.
- [40] E.R. Andresen, S. Sivankutty, V. Tsvirkun, G. Bouwmans, H. Rigneault, Ultrathin endoscopes based on multicore fibers and adaptive optics: a status review and perspectives, *J. Biomed. Opt.* 21 (12) (2016) 121506.
- [41] S. Sharabi, B. Kos, D. Last, D. Guez, D. Daniels, S. Harnof, Y. Mardor, D. Miklavčič, A statistical model describing combined irreversible electroporation and electroporation-induced blood-brain barrier disruption, *Radiol. Oncol.* 50 (2016) 28–38.
- [42] R. Stępień, J. Cimek, D. Pysz, I. Kujawa, M. Klimczak, R. Buczyński, Soft glasses for photonic crystal fibers and microstructured optical components, *Opt. Eng.* 53 (7) (2014) 071815.
- [43] N. Gamper, J.D. Stockand, M.S. Shapiro, The use of Chinese hamster ovary (CHO) cells in the study of ion channels, *J. Pharmacol. Toxicol. Meth.* 51 (3) (2005) 177–185.
- [44] T. Batista Napotnik, D. Miklavčič, In vitro electroporation detection methods - An overview, *Bioelectrochemistry* 120 (2018) 166–182.
- [45] J. Gehl, Electroporation: theory and methods, perspectives for drug delivery, gene therapy and research, *Acta Physiol. Scand.* 177 (4) (2003) 437–447.
- [46] P.T. Vernier, Y. Sun, M.A. Gundersen, Nanoelectropulse-driven membrane perturbation and small molecule permeabilization, *BMC Cell Biol.* 7 (2006) 37.
- [47] P.T. Vernier, Y. Sun, L. Marcu, C.M. Craft, M.A. Gundersen, Nanoelectropulse-induced phosphatidylserine translocation, *Biophys. J.* 86 (6) (2004) 4040–4048.
- [48] E.E. Babiychuk, K. Monastyrskaya, S. Potez, A. Draeger, Blebbing confers resistance against cell lysis, *Cell Death Differ.* 18 (2011) 80–89.
- [49] T.Y. Tsong, Electroporation of cell membranes, *Biophys. J.* 60 (1991) 297–306.
- [50] Y. Zhan, J. Wang, N. Bao, C. Lu, Electroporation of Cells in Microfluidic Droplets, *Anal. Chem.* 81 (2009) 2027–2031.
- [51] J. Ghosh, X. Liu, K.D. Gillis, Electroporation followed by electrochemical measurement of quantal transmitter release from single cells using a patterned microelectrode, *Lab Chip* 13 (11) (2013) 2083–2090.
- [52] J. Dermol, D. Miklavčič, Mathematical models describing Chinese hamster ovary cell death due to electroporation in vitro, *J. Membrane Biol.* 248 (2015) 865–881.
- [53] G. Sersa, M. Cemazar, Z. Rudolf, Electrochemotherapy: advantages and drawbacks in treatment of cancer patients, *Cancer Therapy* 1 (2003) 133–142.
- [54] D. Miklavčič, B. Mali, B. Kos, R. Heller, G. Serša, Electrochemotherapy: from the drawing board into medical practice, *Biomed. Eng. Online* 13 (2014) 29.
- [55] I. Edhemović, E. Breclj, G. Gašljević, M. Marolt Mušič, V. Gorjup, B. Mali, T. Jarm, B. Kos, D. Pavliha, Grčar B. Kuzmanov, M. Čemažar, M. Snoj, D. Miklavčič, E.M. Gadžijev, G. Serša, Intraoperative electrochemotherapy of colorectal liver metastases, *J. Surg. Oncol.* 110 (2014) 320–327.
- [56] D.E. Spratt, E.A. Gordon Spratt, S. Wu, A. DeRosa, N.Y. Lee, M.E. Lacouture, C.A. Barker, Efficacy of Skin-Directed Therapy for Cutaneous Metastases From Advanced Cancer: A Meta-Analysis, *J. Clin. Oncol.* 32 (28) (2014) 3144–3155.
- [57] <https://www.fluigent.com>.
- [58] B. Morova, N. Bavili, Ö. Yaman, B. Yigit, M. Zeybel, M. Aydin, B. Dogan, R. Kasztelanic, D. Pysz, R. Buczynski, A. Kiraz, Design and fabrication of large numerical aperture, high-resolution optical fiber bundles based on novel high-contrast pairs of soft glasses for fluorescence imaging, *Opt. Exp.* 27 (7) (2019) 9502–9515.